3D patient-specific numerical modeling of the soft palate considering adhesion from the tongue

Authors:

Hongliang Liu[a]

Victorien Emile Prot[a]

Bjørn Helge Skallerud[a] (Corresponding author: bjorn.skallerud@ntnu.no, Tel: +47 7355 0303)

[a]Biomechanics Division, Department of Structural Engineering, The Norwegian University of Science and Technology, NTNU, NO-7491 Trondheim, Norway

Manuscripts category: **Original Article**

Keywords: **Cohesive approach; surface tension; patient-specific modeling; numerical simulation; obstructive sleep apnea**

Word counts:

Abstract: 249 Words

Introduction to Conclusion: 3913 Words

3D patient-specific numerical modeling of the soft palate considering adhesion from the tongue

Hongliang Liu[a], Victorien Emile Prot[a], Bjørn Helge Skallerud[a,*]

[a]*Biomechanics Division, Department of Structural Engineering, The Norwegian University of Science and Technology, NTNU, NO-7491 Trondheim, Norway*

Abstract

Collapse of the soft palate in the upper airway causes obstructive sleeping problem. A comprehensive numerical simulation of the soft palate contributes to providing useful information to the clinical study. The adhesion effect from the tongue still remains to be investigated, and no cohesive simulation for the surface tension has been presented. In this study, the traction-separation cohesive approach was addressed to describe the adhesion effect from the surface tension of the lining liquid between the soft palate and the tongue. According to pull-off experimental tests of human lining liquid from the oral surface of the soft palate, the corresponding cohesive properties, including the critical normal traction stress and the failure separation displacement, were obtained. The 3D patient-specific soft palate geometry was accounted for, based on one specific patient's computed tomography (CT) images. The calculation results showed that influence of the adhesion from the tongue surface on the global response of the soft palate depends on the length ratio between the cohesive length and the soft palate length. When the length of the cohesive zone was smaller than half of the soft palate length, the adhesion's influence was negligible. When the adhesion length was larger than 70 percent of soft palate length, the adhesion force contributes to preventing the soft palate from collapsing towards to the pharynx wall, i.e. the closing pressure was more negative than in the no adhesion case. These results may provide useful information to the clinical treatment of OSA patients.

Keywords: Cohesive approach, surface tension, patient-specific modeling, numerical simulation, obstructive sleep apnea

1. Introduction

For obstructive sleep apnea (OSA) patients, the collapse of the soft palate in the upper airway is one of the main causes of breathing stops. Typically, when patients sleep with their mouths closed, the collapse of the soft palate towards the pharynx wall will block normal airflow in the upper airway (Fig .1). The direct reason for the collapse of the soft palate is attributed to the negative pressure that may be caused by the narrowing upper airway. Biomechanical behavior of the soft palate in response to the negative pressure including the collapse will, in turn, have an influence on the pressure distribution of the upper airway and the air flow velocity. Hence,

*Corresponding author
Email address: bjorn.skallerud@ntnu.no (Bjørn Helge Skallerud)

a comprehensive biomechanics study of the soft palate in the upper airway contributes to the clinical research of OSA and provides input to improved understanding of the phenomenon.

Numerical modeling of the soft palate has been addressed to investigate the soft palate's response to the airway pressure. Berry et al. (1999) presented an approximate 2-dimensional (2D) cantilever model of the soft palate and the collapse shape of the soft palate was obtained. Malhotra et al. (2002) employed a 2D planar model to investigate the closing pressure of the soft palate. In their finite element (FE) model, based on clinical results, a fitted Young's modulus value of soft palate was obtained. Sun et al. (2007) presented the movement of soft palate during breathing with a simplified 3D model. Wang et al. (2012) presented a fluid-solid interaction numerical simulation for the upper airway, including the soft palate. Inouye et al. (2015) showed a computational model for the soft palate closure to simulate the cleft palate repair. These research works showed a basic method for numerical modeling of the soft palate. On the other hand, according to Fig. 1, contact between the soft palate and the tongue is observed. The surface tension of the upper airway mucosal lining liquid was shown to produce an influence on the upper airway collapsibility (Kirkness et al., 2003). The surface tension generated by the mucosal lining liquid between the soft palate and the tongue produces an adhesion force to prevent the soft palate debonding from the tongue. To the authors' knowledge, investigation of this surface tension has not been addressed in the literature. Therefore, a numerical method was developed to assess the adhesion's influence on the soft palate's behavior. In addition, the adhesion investigation also can contribute to evaluating the influence of the upper airway humidity (especially the dry throat) on the global response of the soft palate.

Surface tension is due to the elasticity of a fluid surface obtaining the least surface area. Modeling of the surface tension for fluids has been presented in the literature, such as a continuum method (Brackbill et al., 1992) and additive-nonadditive modeling method (Van Oss et al., 1988). When a solid body, such as a soft tissue, is in contact with a liquid surface, the adhesion is a result of the corresponding positive adhesion energy (Jensen et al., 2015). For the liquid, the surface energy is often described to be equal to the surface tension (Shen et al., 2015). Studies of the adhesion between soft materials and liquids are mainly described with surface indentation models, using a spherical indenter and a flat substrate (Hui et al., 2015; Watson et al., 2015; Chakrabarti and Chaudhury, 2013). In addition, contact mechanics theories such as Johnson-Kendall-Roberts (JKR) (Johnson et al., 1971) and Derjaguin-Muller-Toporov (DMT) (Derjaguin et al., 1994) have been used to describe the relation between the external separation force and the adhesion energy, which corresponds to the surface tension (Xu et al., 2014; Jensen et al., 2015; Rasuli et al., 2010).

On the other hand, a cohesive zone approach combined with the finite element method has been presented in the simulations to solve fracture mechanics problems, such as the needle insertion (Oldfield et al., 2013) and failure of the brittle rocks (Gui et al., 2016). In addition, the cohesive models have been applied to various biomechanical problems, such as simulation of cell-matrix adhesion described by Cóndor and García-Aznar (2017), arterial dissection presented by Gasser and Holzapfel (2006) and Noble et al. (2017), soft material tearing provided by Bhattacharjee et al. (2013).

In order to address the adhesion between the soft palate and the tongue due to the lining liquid in the numerical simulation, we used the cohesive approach to simulate the surface tension, which has not been presented in the literature. An OSA patient's CT images were used to reconstruct the soft palate geometry. Corresponding cohesive properties was obtained based on experimental data. Moreover, investigation of different cohesive properties of the lining liquid may provide improved understanding of how the humidity of the upper airway influences the soft palate collapse and how to improve treatment for OSA patients.

2. Methods

2.1. Cohesive approach

In the FE code ABAQUS, adhesion modeling of the bonded bodies can be achieved with cohesive elements and a traction-separation model for a specifically defined cohesive layer. The relationship between the traction and the separation is presented as Fig. 2. Assuming that the normal direction (debonding direction) of the cohesive layer is direction 1, and directions 2 and 3 denote the orthogonal in-plane directions, the nominal traction stress $\mathbf{t}$ is described as $[t_i] = [t_1, t_2, t_3]^{\mathrm{T}}$. The initial constitutive thickness of the cohesive layer is denoted by T_0. According to the separation displacement $\boldsymbol{\delta}$, the nominal strain is calculated as $\boldsymbol{\epsilon} = \boldsymbol{\delta}/T_0$. In ABAQUS, the default value for T_0 is set to be 1, this ensures that the nominal strain is equal to the separation. The detailed description is reported in ABAQUS analysis user's guide (ABAQUS, 2014). When the separation displacement δ increases to the damage initiation value δ_{i} (see Fig. 2), the traction stress reaches the maximum value t_{c}, and the degradation process begins. In the degradation process, the traction stress decreases gradually to 0 as δ increases towards δ_{f}, which is defined as the separation at failure.

In this study, we mainly considered the normal direction's mechanical behavior, and a linear elastic stiffness E was used until the traction stress reaches the critical level (the initial stage). The elastic behavior is described as

$$t_1 = E\epsilon_{11} = E\delta, \tag{1}$$

where δ is the separation in the normal direction of the cohesive layer. Additionally, in the degradation process, a scalar damage variable D is used to define the traction stress within ABAQUS (ABAQUS, 2014)

$$t_1 = (1 - D)E\delta, \tag{2}$$

where D has an initial value 0 and increases to 1 in the end of the degradation process (failure). In this study, the linear degradation process was considered (see Fig. 2).

2.2. Pull-off test of upper airway lining liquid

In the cohesive approach, two important values are needed when investigating the adhesion of the mucosal lining liquid between the soft palate and tongue. One is the normal direction's critical traction stress t_{c} defined

as the critical value for damage initiation, and the other one is the failure separation displacement δ_{f} in the normal direction of the cohesive layer. Based on the surface tension test of the upper airway lining liquid provided by Kirkness et al. (2005), we can determine these two values. In their experimental test, the lining liquid's thickness was initially equal to 21 μm. This is close to the normal human lining liquid's thickness of 26.4 μm (Lee et al., 2002) on the soft palate's oral surface. In addition, the pull-off force separating the adhesion was calculated in the experimental test as

$$F = 2\pi R\gamma(2cos\theta + sin(\theta + \phi)), \tag{3}$$

where γ is the surface tension, which was tested to be 56.1 mNm^{-1} for the lining liquid between the soft palate and the tongue. R, θ and ϕ are geometry constants measured in the experimental test, see Fig. 3. In their pull-off test, two cylindrical silica discs were stacked together with the axes perpendicular to each other. The lining liquid from the upper airway was coated on the disc's surface and generated an annulus, which can be shown as in Fig. 3. The detailed description is provided in Kirkness et al. (2005). The values for the geometrical constants are: $R = 20$ mm and $\theta = \phi = 5°$. Based on the obtained surface tension and Eq. (3), the pull-off force can be calculated to be 15.27 mN.

Based on the obtained pull-off force, we calculated the critical traction stress t_{c} (Fig. 2) in the normal direction as

$$t_{\mathrm{c}} = \frac{F}{A_0}, \tag{4}$$

where A_0 is the contact area of the tested lining liquid surface and F is the obtained pull-off force. As shown in Fig. 3, the contact area of the lining liquid in the test is calculated to be $A_0 = \pi r^2$. Since the radius R was set to be 20 mm and the angle ϕ was measured to be 5° (Kirkness et al., 2005), the radius of the contact zone r in Fig. 3 is 1.74 mm. Then, the contact area A_0 in Eq. (4) was obtained as 9.51 mm^2, and the critical traction stress was calculated as 1.61 kPa.

On the other hand, in the experimental pull-off test, a jump apart of the two discs stacked together with the lining liquid was observed. This jump displacement was named D. Relating the stiffness k of the spring that was used in the experimental test to the pull-off force, the jump apart displacement was calculated as:

$$D = F/k. \tag{5}$$

The detailed description was reported in Kirkness et al. (2005). The jump apart displacement D was calculated to be 0.57 mm, based on Eq. (5). In this study, we assumed the failure separation δ_{f} is equal to this jump apart displacement observed in the experimental test.

Hence, the two key values for the cohesive approach (the critical traction stress t_{c} and the failure separation displacement δ_{f}) are obtained. Since the separation evolves in the normal direction, for the cohesive approach, the failure separation displacement δ_{f} is only needed to be set in the normal direction.

Additionally, we assumed the human lining liquid has an isotropic cohesive property. Then, we used the same elastic stiffness E as in Eq. (1) for all three directions in the simulation. Based on the obtained critical traction stress t_c and the failure separation δ_f in the normal direction, we only needed to determine the initial linear elastic stiffness E, which is related to the damage initial separation δ_i. δ_i has a limited influence on the global response of the separation of two bonded bodies, such as the soft palate and the tongue. The strain energy represented as the area underneath the curve shown in Fig. 2 will be the same for different choices of δ_i. We set δ_i to be 0.01 mm in this study to address the adhesion simulation of the soft palate.

In order to ensure our numerical model gives the same pull-off force as in the experimental test, a simplified FE model was created to mimic the pull-off test of the human upper airway mucosal lining liquid. According to the numerical simulation result, the obtained pull-off pressure corresponds with the experimental test value 1.61 kPa.

In addition, the influence of E on the calculation of the critical traction pressure was checked, showing that it was very limited. We tested two more cases: $\delta_i = 0.1$ and $\delta_i = 0.2$. The obtained critical pull-off pressure is the same as for $\delta_i = 0.01$. Moreover, since the normal human lining liquid thickness on the oral surface of the soft palate was measured to be 26.4 μm (Lee et al., 2002), we set the thickness of the lining liquid in the soft palate simulation to be 26.4 μm. As the test results for different thicknesses showed no difference (Kirkness et al., 2005), the obtained cohesive properties in the description above were used in the following simulations for the soft palate.

2.3. Numerical modeling for the soft palate and tongue

2.3.1. 3D patient-specific geometry

Recently, computational 3D modeling based on CT or MR images has been applied successfully for studies of the upper airway (Sera et al., 2015; Sung et al., 2006). In the current study, based on one specific patient's CT images, we obtained the 3D geometry in ABAQUS. Usage of the images was approved by the Norwegian Regional Committee for Medical Research Ethics (REK) and was registered in Clinicaltrials.gov. (NCT01282125). The detailed description for the geometry modeling has been presented in our previous work Liu et al. (2018). In addition, we simplified the boundary between the tongue and the soft palate as a straight line, which contributes to obtaining an efficient numerical cohesive simulation. Moreover, to simplify the simulation, as shown in Fig. 4, the whole tongue was not reconstructed. The cohesive part of the tongue was modeled as a 20 mm thickness brick and the length of the cohesive zone was measured to be 17 mm based on the specific patient's CT image. The thickness of the cohesive layer was set to be 26.4 μm (Lee et al., 2002). Additionally, since the patient-specific CT images was scanned when the patient was lying down with the supine position, the influence of the gravity of the tongue was considered in the remaining numerical simulation.

2.3.2. *Material properties and boundary conditions*

A neo-Hookean hyperelastic model was employed. The strain-energy function reads:

$$\Psi(\bar{I}_1, J) = \underbrace{c(\bar{I}_1 - 3)}_{\text{isochoric}} + \underbrace{\frac{1}{D_1}(J-1)^2}_{\text{volumetric}}. \tag{6}$$

Here, c, D_1 are material parameters derived from the Young's modulus E and Poisson's ratio ν with the following relations (Berry et al., 1999):

$$c = \frac{E}{4(1+\nu)}, \quad D_1 = \frac{6(1-2\nu)}{E}. \tag{7}$$

The value of the Young's modulus for the soft palate was determined according to an in vivo magnetic resonance elastography measurement of the soft palate provided by Cheng et al. (2011). Assuming the Poisson's ratio value to be 0.49, the Young's modulus was calculated to be 7.539 kPa, based on the measured shear modulus 2.53 kPa. In addition, the neo-Hookean model was also used to define the material property of the tongue. According to the in vivo measured shear modulus 2.67 kPa by Cheng et al. (2011), the Young's modulus of the tongue was calculated to be 7.957 kPa with a Poisson's ration of 0.49. Moreover, for the cohesive layer, the cohesive properties in Section 2.2 were used, including the obtained critical traction stress $t_{\mathrm{c}} = 1.61\mathrm{kPa}$ and the failure separation $\delta_{\mathrm{f}} = 0.57\mathrm{mm}$.

The boundary conditions for the soft palate were set as in Fig. 5, and the bottom of the tongue shown in Fig. 4 was also constrained. Finally, since the collapse of the soft palate in the negative pressure field is one of the main reasons to cause OSA, we applied a uniformly distributed pressure, corresponding to the pressure difference between the anterior and posterior sides of the soft palate (Fig. 4), on the surface where the soft palate contacts with the airway (Fig. 5).

$$P_{\mathrm{negative}} = P_{\mathrm{posterior}} - P_{\mathrm{anterior}}. \tag{8}$$

When the negative pressure develops, the soft palate will have a posterior oblique deformation. If the negative pressure is large enough, the soft palate will stick to the pharynx wall. Then, the OSA occurs. We call this critical negative pressure the closing pressure. However, the adhesion force from the mucosal lining liquid between the soft palate and the tongue will act against this posterior oblique deformation of the soft palate. Therefore, the investigation of the global response of the soft palate considering the adhesion effect contributes to obtaining physiological simulation results.

2.3.3. *Mesh convergence study*

The 3D patient-specific soft palate model was meshed with four noded hybrid tetrahedral elements (C3D4H ABAQUS type). A -5 cm H2O negative pressure was applied and the neo-Hookean model with the aforementioned property data of the soft palate was assigned to the 3D patient-specific model. As shown in Fig. 6, four mesh densities were tested with 139 338, 397 716, 651 742 and 852 870 elements, corresponding to Mesh 1,

Mesh 2, Mesh 3 and Mesh 4, respectively. The difference for the critical parameter between Mesh 3 and Mesh 4 was 0.7% (Fig. 6). Therefore, considering the simulation accuracy and computational time efficiency, we used a mesh with the size of Mesh 3 in the remaining simulation of this paper. Meanwhile, the cohesive element with the same mesh size was assigned to the cohesive layer, and the tongue was also meshed with the size of Mesh 3 and the eight noded hybrid elements (C3D8H ABAQUS type) were addressed.

3. Results

The collapse of the soft palate in the upper airway and the failure of the adhesion with respect to the cohesive layer could be observed directly with the 3D patient-specific geometry as shown in Fig. 6. Additionally, in order to present the global response of the soft palate, we used the norm of the displacement of point A to quantify the inclination displacement of the posterior surface of the soft palate, see Fig. 7. When point A makes contact with the pharynx wall, the corresponding negative pressure was set to be the closing pressure, which was regarded as a critical parameter to evaluate the global response of the soft palate. The detailed calculation results are shown as Fig. 8. Based on the simulation results, for this specific patient, we found that the influence of adhesion from the lining liquid between the soft palate and tongue on the global response of the soft palate is negligible. The closing pressure, considering the adhesion effect, was calculated to be -5.56 cm H_2O. In the no adhesion case, the closing pressure was -5.54 cm H_2O. This is reasonable, considering the length of the cohesive layer was measured to be only half the length of the soft palate, while point A locates at the distal part of the soft palate.

In order to have a more comprehensive study of the adhesion effect, we investigated 18 patients' CT images and found different contact types. We divided them into 4 adhesion types (Table 1), based on the ratio between the adhesion length and the soft palate length, including below 50%, 50%-70%, above 70% and tip adhesion types. For simplicity, we did not create all these patients' 3D geometry model. Instead, we extended the length of the cohesive layer (shown in Fig. 4) in the created patient-specific model. The length of the tongue model was also extended following the extension of the cohesive layer. In addition, for the tip adhesion case, we only modeled the tip part's contact, and the anterior part's contact between the soft palate and the tongue was neglected, because for a short contact length the adhesion influence is very limited, according to Fig. 8 (A). The global responses of soft palate versus the negative pressure for each contact type are shown in Fig. 8. The closing pressure for each case are reported in Table 1. According to the simulation results, the adhesion effect is observed to be strengthened following the increase of the adhesion length. Failure of the adhesion (see Fig. 7) occurs when the adhesion length is larger than 70 percent of the soft palate. Additionally, when the adhesion failure happens, a step-increase of the norm of displacement of point A is presented, corresponding to the decrease of the traction stress during the degradation process (Fig. 2). Moreover, the closing pressure is also observed to become more negative following the increase of the adhesion length. We also used the created patient-specific 3D geometry for the simulation of the tip adhesion case.

We used the critical traction stress 1.61 kPa in the above simulations, based on the pull-off experiment test. The critical traction stress relates directly to the adhesion strength. This motivates us to investigate another

case for evaluating the influence of changing the critical traction stress on the global response of the soft palate. A smaller critical traction stress of magnitude 0.5 kPa was considered. The adhesion length was set to be 70 percent of the soft palate. Using the same initial separation displacement for damage ($\delta_i = 0.01$), the initial linear elastic stiffness was calculated to be 50 kPa. The comparison between these two kinds of critical traction stresses is shown in Fig. 9. According to the calculation results, different global responses of soft palate evolve, and the closing pressure for the smaller critical traction stress case is less negative than the larger one. Moreover, it is obvious that the adhesion failure starts earlier for the smaller critical traction stress case. This shows that the critical traction stress has a significant influence on the adhesive behavior.

4. Discussion and conclusion

The adhesion from the mucosal lining liquid on the soft tissue's surface has an influence on the biomechanical behavior of the corresponding soft tissue. This is presented in the above simulations for the deformation of the soft palate, accounting for the adhesion due to the lining liquid between the soft palate and tongue. Based on the experimental pull-off test of the human lining liquid from the oral surface of soft palate (Kirkness et al., 2005), using the traction-separation cohesive approach, a 3D patient-specific numerical simulation considering the adhesion effect was achieved. The simulation results show that the adhesion strengthening effect depends on the contact area between the soft palate and the tongue. When the contact length is smaller than half of the soft palate length, the adhesion's influence on the global response of the soft palate was negligible. For a contact length larger than 70 percent of the length of the soft palate, the adhesion leads to a more negative closing pressure for the soft palate, but this improvement rate is moderate. Kirkness et al. (2003) showed that decreasing the surface tension of the upper airway lining liquid contributes to reducing the upper airway collapsibility. Their research focused on the collapse of the whole upper airway, which can be treated as a tube. Our study investigated the adhesion between the soft palate and the tongue, and the surface tension of the lining liquid on the posterior surface of the soft palate was not accounted in the numerical simulation. Therefore, we conclude that the adhesion between the soft palate and the tongue prevents the soft palate from collapse. A further investigation of the pharyngeal lining liquid's surface tension working on the soft palate's posterior surface remains to be addressed.

The strength of the adhesion depends mainly on the critical traction stress in the normal direction. We obtained this value from the pull-off experiment test. Some patients may suffer from dry throat (lining liquid humidity change), and the adhesion from the tongue may be weaker than for healthy people. We investigated a weaker adhesion case where the critical traction stress was set to be 0.5 kPa, which is lower than the healthy people's 1.61 kPa. The comparison result showed that the closing pressure is less negative for the weaker adhesion case. Whether the humidity degree of the upper airway has a direct influence on the critical traction stress of the lining liquid remains to be validated in the further work. Our simulation results point out that increasing the adhesion force from tongue can make the closing pressure of soft palate more negative and may improve the obstructive sleeping condition for OSA patients. Moreover, we used the failure separation with

0.57 mm. In the real case, small variation of this value may be found. We also investigated another case with failure separation of 0.5 mm. The results showed a small difference between these two cases' calculations. This indicates that the variation of the failure separation δ_f in a small range has a limited influence on the global response of the soft palate.

In our simulation, only the passive condition was considered, and the neuromuscular activation effect from palatal muscle fibers was neglected, considering the patients' activation level is defective (McGinley et al., 2008). Moreover, in order to simplify the calculation, we applied the negative pressure as a uniformly distributed load. However, this is not the case in reality. Therefore, fluid-structure interaction analysis may be employed in order to predict a more realistic pressure distribution when the large deformation problem is considered. This will be a task in the further studies of the soft palate. In addition, we defined the closing pressure as the negative pressure that make the point A contacts the pharynx wall. This is an approximate definition since the soft palate is not fully collapsed. We used this approximate method to get a consistence result when comparing different simulation cases. In addition, we simplified the geometry between the soft palate and the tongue as a plane, which contributes to efficient cohesive simulation. Moreover, we simplified the geometry of the tongue to be a block body. In the further study, more physiological geometry model is needed to achieve more realistic simulation results. Additionally, for different cohesive length cases' simulation, we used only one patient-specific geometry. The patient-specific model for each case will be created in our next step work that achieves more physiological simulation results.

Based on the pull-off test of the human lining liquid, using the traction-separation cohesive approach, we provide a method for numerical modeling of the soft palate, considering the adhesion effect from the mucosal lining liquid. The adhesion effect is evaluated to have an influence on the global response of soft palate, but this influence in terms of the change of closing pressure is moderate. The cohesive simulation gives input to the clinical research on how the adhesion effect of the upper airway lining liquid influences the biomechanical behavior of the soft palate. For example, keeping the optimal humidity in the the OSA patients' throat may be considered as a method to reduce the soft palate collapse tendency and improve the patients' sleep condition.

Conflict of interest statement

The authors declare that they have no conflict of interest.

Acknowledgements

The project has been funded in part from a grant from the Research Council of Norway and a grant from NTNU, Norway.

References

ABAQUS, 2014. Abaqus Analysis User's Guide: version 6.14. SIMULIA.

Berry, D.A., M., J.B., Kuehn, D.P., 1999. A finite element model of the soft palate. The Cleft Palate-Craniofacial Journal 36, 217–223.

Bhattacharjee, T., Barlingay, M., Tasneem, H., Roan, E., Vemaganti, K., 2013. Cohesive zone modeling of mode i tearing in thin soft materials. Journal of the Mechanical Behavior of Biomedical Materials 28, 37 – 46.

Brackbill, J.U., Kothe, D.B., Zemach, C., 1992. A continuum method for modeling surface tension. Journal of Computational Physics 100, 335 – 354.

Chakrabarti, A., Chaudhury, M.K., 2013. Direct measurement of the surface tension of a soft elastic hydrogel: Exploration of elastocapillary instability in adhesion. Langmuir 29, 6926–6935.

Cheng, S., Gandevia, S.C., Green, M., Sinkus, R., Bilston, L.E., 2011. Viscoelastic properties of the tongue and soft palate using mr elastography. Journal of biomechanics 44, 450–454.

Cóndor, M., García-Aznar, J.M., 2017. A phenomenological cohesive model for the macroscopic simulation of cell–matrix adhesions. Biomechanics and Modeling in Mechanobiology , 1–18.

Derjaguin, B.V., Muller, V.M., Toporov, Y.P., 1994. Effect of contact deformations on the adhesion of particles. Progress in Surface Science 45, 131 – 143.

Gasser, T.C., Holzapfel, G.A., 2006. Modeling the propagation of arterial dissection. European Journal of Mechanics-A/Solids 25, 617–633.

Gui, Y., Bui, H.H., Kodikara, J., Zhang, Q., Zhao, J., Rabczuk, T., 2016. Modelling the dynamic failure of brittle rocks using a hybrid continuum-discrete element method with a mixed-mode cohesive fracture model. International Journal of Impact Engineering 87, 146 – 155. SI: Experimental Testing and Computational Modeling of Dynamic Fracture.

Hui, C., Liu, T., Salez, T., Raphael, E., Jagota, A., 2015. Indentation of a rigid sphere into an elastic substrate with surface tension and adhesion. Proceedings of the Royal Society of London A: Mathematical, Physical and Engineering Sciences 471.

Inouye, J.M., Pelland, C.M., Lin, K.Y., Borowitz, K.C., Blemker, S.S., 2015. A computational model of velopharyngeal closure for simulating cleft palate repair. Journal of Craniofacial Surgery 26, 658–662.

Jensen, K.E., Sarfati, R., Style, R.W., Boltyanskiy, R., Chakrabarti, A., Chaudhury, M.K., Dufresne, E.R., 2015. Wetting and phase separation in soft adhesion. Proceedings of the National Academy of Sciences 112, 14490–14494.

Johnson, K.L., Kendall, K., Roberts, A.D., 1971. Surface energy and the contact of elastic solids. Proceedings of the Royal Society of London A: Mathematical, Physical and Engineering Sciences 324, 301–313.

Kirkness, J.P., Christenson, H.K., Wheatley, J.R., Amis, T.C., 2005. Application of the 'pull-off' force method for measurement of surface tension of upper airway mucosal lining liquid. Physiological Measurement 26, 677.

Kirkness, J.P., Madronio, M., Stavrinou, R., Wheatley, J.R., Amis, T.C., 2003. Relationship between surface tension of upper airway lining liquid and upper airway collapsibility during sleep in obstructive sleep apnea hypopnea syndrome. Journal of Applied Physiology 95, 1761–1766.

Lee, S.K., Lee, S.W., Chung, S.C., Kim, Y.K., Kho, H.S., 2002. Analysis of residual saliva and minor salivary gland secretions in patients with dry mouth. Archives of oral biology 47, 637–641.

Liu, H., Moxness, M.H.S., Prot, V.E., Skallerud, B.H., 2018. Palatal implant surgery effectiveness in treatment of obstructive sleep apnea: A numerical method with 3d patient-specific geometries. Journal of Biomechanics 66, 86–94.

Malhotra, A., Huang, Y., Fogel, R.B., Pillar, G., Edwards, J.K., Kikinis, R., Loring, S.H., White, D.P., 2002. The male predisposition to pharyngeal collapse. American Journal of Respiratory and Critical Care Medicine 166, 1388–1395.

McGinley, B.M., Schwartz, A.R., Schneider, H., Kirkness, J.P., Smith, P.L., Patil, S.P., 2008. Upper airway neuromuscular compensation during sleep is defective in obstructive sleep apnea. Journal of Applied Physiology 105, 197–205.

Noble, C., Sluis, O., Voncken, R.M.J., Burke, O., Franklin, S.E., Lewis, R., Taylor, Z.A., 2017. Simulation of arterial dissection by a penetrating external body using cohesive zone modelling. Journal of the Mechanical Behavior of Biomedical Materials 71, 95 – 105.

Oldfield, M., Dini, D., Giordano, G., y. Baena, F.R., 2013. Detailed finite element modelling of deep needle insertions into a soft tissue phantom using a cohesive approach. Computer Methods in Biomechanics and Biomedical Engineering 16, 530–543.

Rasuli, R., zad, A.I., Ahadian, M.M., 2010. Mechanical properties of graphene cantilever from atomic force microscopy and density functional theory. Nanotechnology 21, 185503.

Sera, T., Uesugi, K., Yagi, N., Yokota, H., 2015. Numerical simulation of airflow and microparticle deposition in a synchrotron micro-ct-based pulmonary acinus model. Computer Methods in Biomechanics and Biomedical Engineering 18, 1427–1435.

Shen, J., He, Y., Wu, J., Gao, C., Keyshar, K., Zhang, X., Yang, Y., Ye, M., Vajtai, R., Lou, J., Ajayan, P.M., 2015. Liquid phase exfoliation of two-dimensional materials by directly probing and matching surface tension components. Nano Letters 15, 5449–5454.

Sun, X., Yu, C., Wang, Y., Liu, Y., 2007. Numerical simulation of soft palate movement and airflow in human upper airway by fluid-structure interaction method. Acta Mechanica Sinica 23, 359–367.

Sung, S.J., Jeong, S.J., Yu, Y.S., Hwang, C.J., Pae, E.K., 2006. Customized three-dimensional computational fluid dynamics simulation of the upper airway of obstructive sleep apnea. The Angle Orthodontist 76, 791–799.

Van Oss, C.J., Good, R.J., Chaudhury, M.K., 1988. Additive and nonadditive surface tension components and the interpretation of contact angles. Langmuir 4, 884–891.

Wang, Y., Wang, J., Liu, Y., Yu, S., Sun, X., Li, S., Shen, S., Zhao, W., 2012. Fluid–structure interaction modeling of upper airways before and after nasal surgery for obstructive sleep apnea. International journal for numerical methods in biomedical engineering 28, 528–546.

Watson, G.S., Green, D.W., Schwarzkopf, L., Li, X., Cribb, B.W., Myhra, S., Watson, J.A., 2015. A gecko skin micro/nano structure-a low adhesion, superhydrophobic, anti-wetting, self-cleaning, biocompatible, antibacterial surface. Acta Biomaterialia 21, 109 – 122.

Xu, X., Jagota, A., Hui, C., 2014. Effects of surface tension on the adhesive contact of a rigid sphere to a compliant substrate. Soft Matter 10, 4625–4632.

Table and figure captions

Table 1. The closing pressure for different length ratio cases and the patients' distribution for these cases.

Length ratio	No adhesion	Below 50%	50% – 70%	Above 70%	Tip adhesion
Closing pressure ($-$cm H_2O)	5.54	5.54 – 5.56	5.56 – 6.16	6.16 – 7.44	5.96
Number of patients	0	4	4	6	4

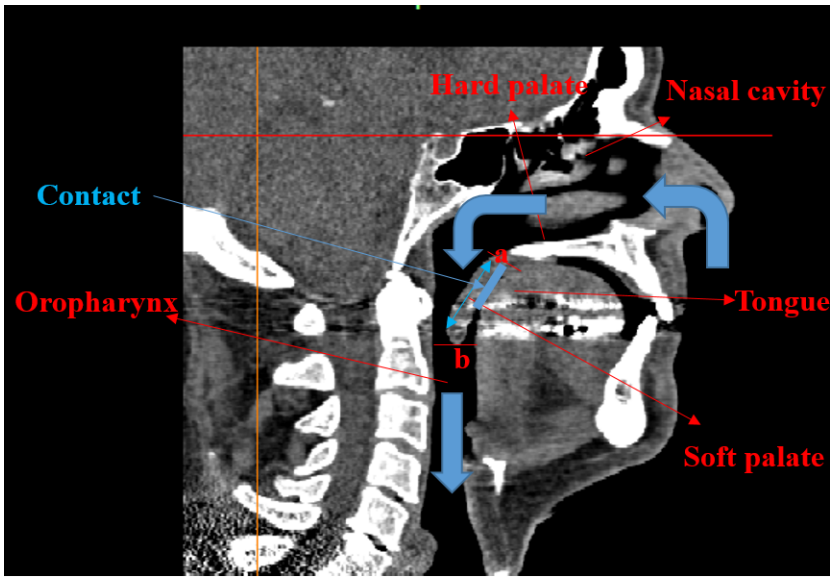

Fig. 1. CT image of the upper airway in the sagittal midsection. In the breathing process with mouth closed, the air flow comes into the lung through the nasal cavity, pharynx. The soft palate locates in the top part of the pharynx, connecting to the hard palate. We use "a" and "b" markers to have a clear description of the soft palate's position in the following. The "a" section means the side between the soft palate and the hard palate, the "b" section means the bottom edge of the soft palate tip. In addition, the contact between the soft palate and tongue is marked (blue short line).

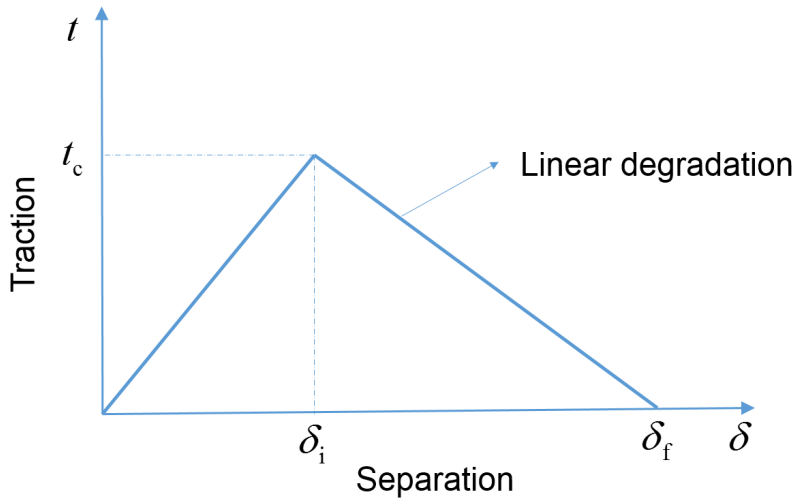

Fig. 2. Traction-separation model for the cohesive approach, the damage initial separation and failure separation are presented.

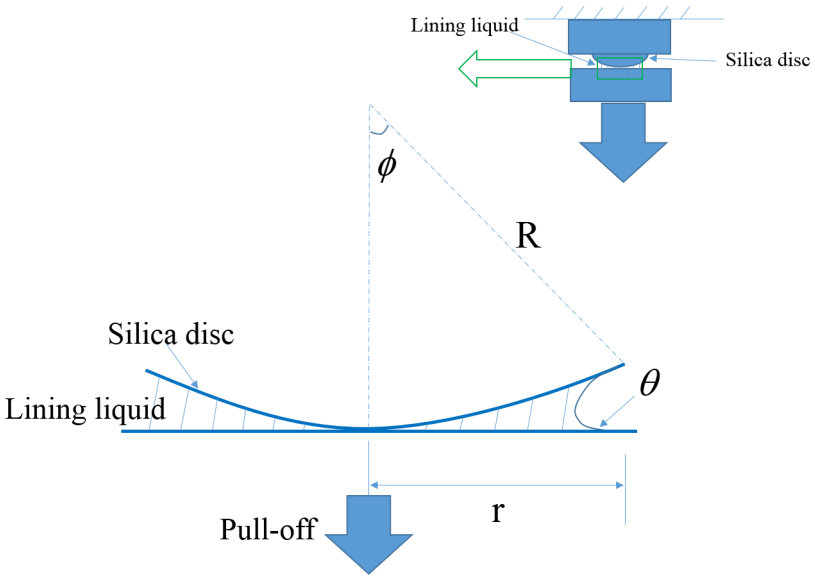

Fig. 3. The schematic of the pull-off test of human upper airway lining liquid according to Kirkness et al. (2005). The top disc is constrained and the lower disc is pulled down with a spring that can measure the pull-off force. The angle θ represents the contact angle between the liquid and the lower disc and angle ϕ is an angular measurement of the size of the liquid annulus, which can be used to calculated the contact area between the disc and lining liquid.

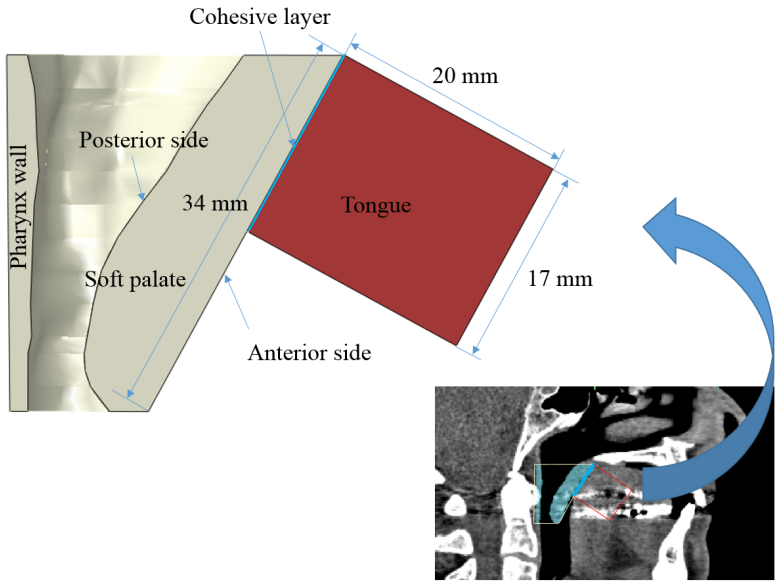

Fig. 4. Obtained patient-specific geometry model that was used to investigate the influence of the adhesion from the lining liquid between the soft palate and tongue on the global response of the soft palate in the sagittal midsection view. The length of the soft palate is 34 mm and the contact length between the soft palate and tongue is 17 mm.

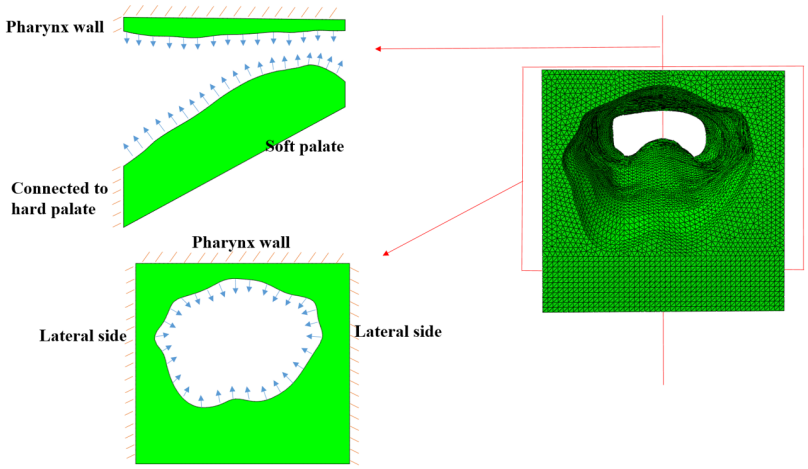

Fig. 5. Boundary conditions for the 3D patient-specific model: the external surface of the pharynx wall, the lateral sides and the side connected to the hard palate were constrained in all directions. The left-top figure is the in the view from right to left and the left-bottom figure is in the view looking inside.

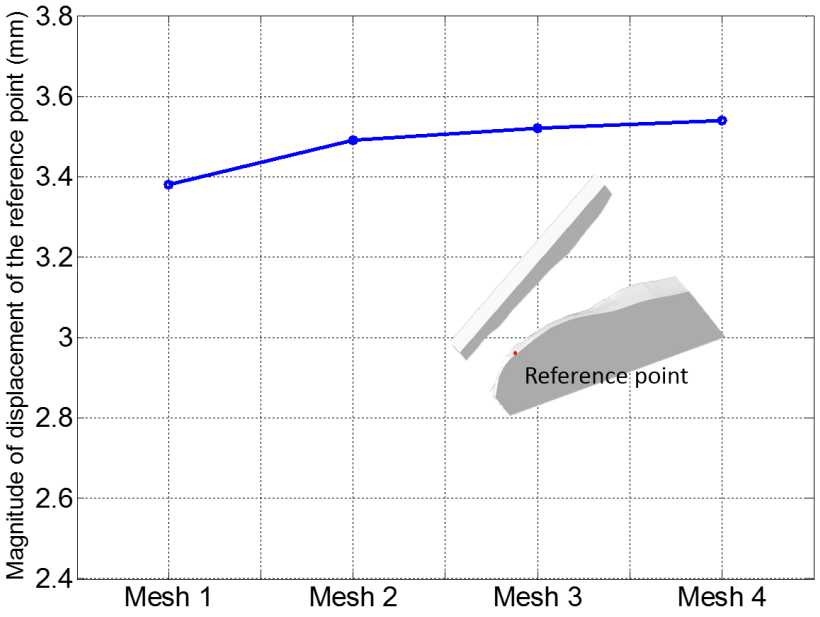

Fig. 6. Mesh convergence analysis result. The displacement of the reference point in the midsection of the soft palate's posterior surface was chosen as a critical parameter and compared for different mesh densities.

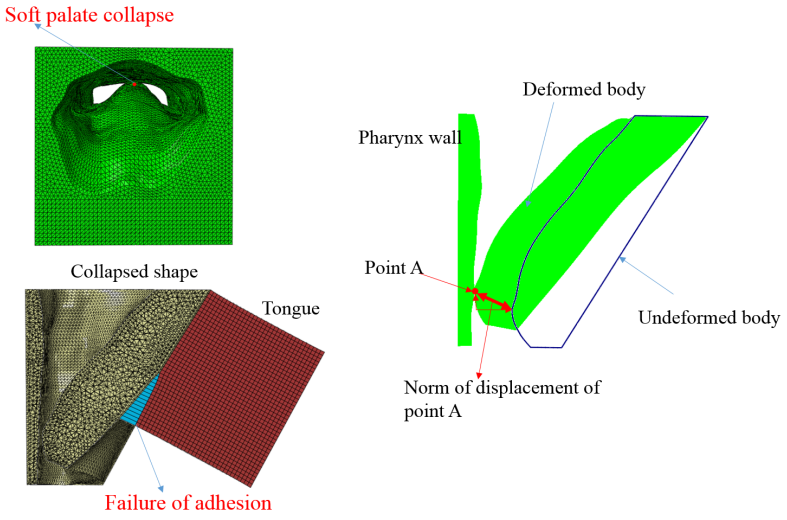

Fig. 7. Collapsed deformation of the 3D patient-specific soft palate model (view from the nasopharynx cavity), the failure of the adhesion for the cohesive layer (70% soft palate length for the cohesive layer) in the sagittal midsection view and the definition of point A and of the norm of its displacement for the 3D patient-specific model in the sagittal midsection plane. Point A was defined to be the first point of the soft palate posterior surface to be in contact with the pharynx wall in the sagittal midsection plane. The displacement of point A was used to represent the inclination displacement of soft palate tip's posterior surface.

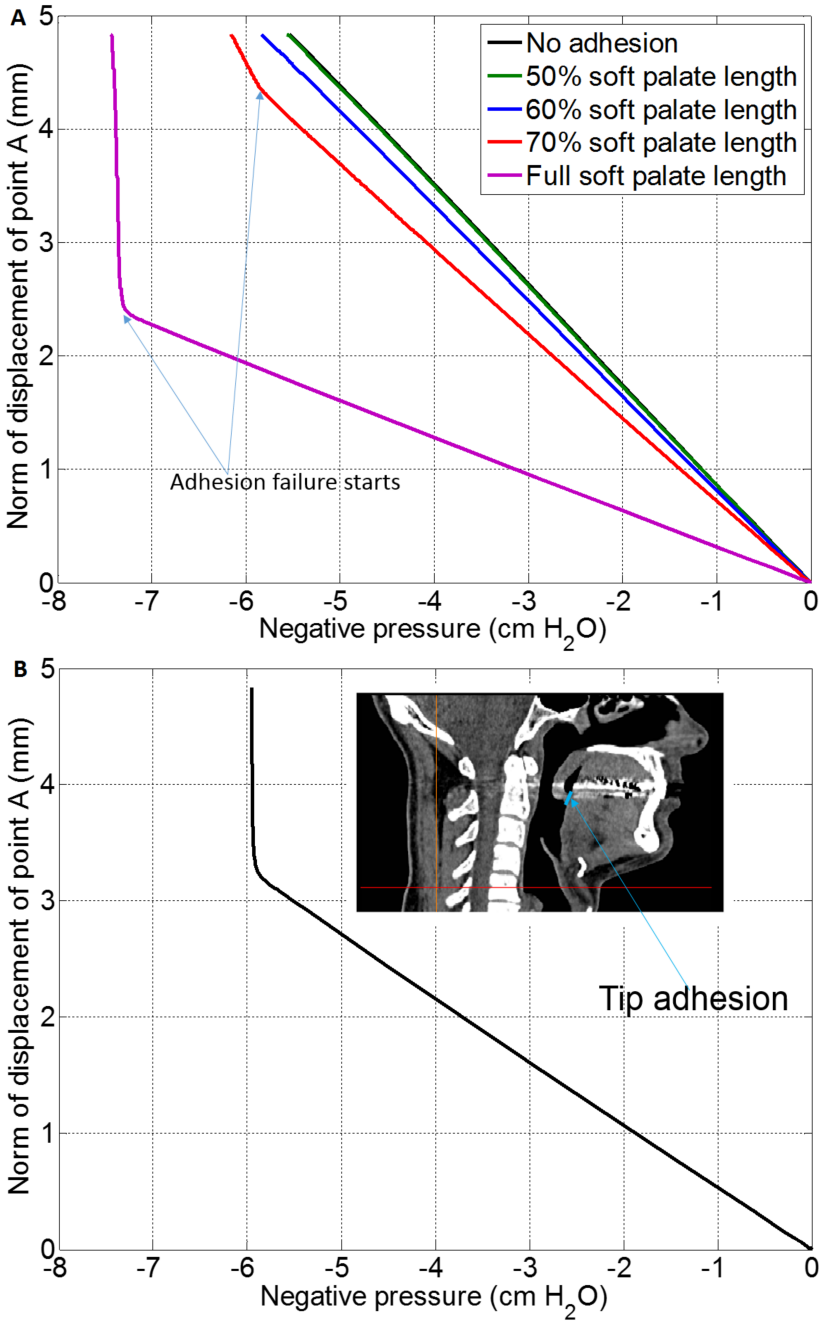

Fig. 8. (A) Negative pressure against the norm of displacement of point A for the 3D patient-specific adhesion model, including different contact length cases except the tip adhesion case. (B) Negative pressure against the norm of displacement of point A for the tip adhesion case. A step-increasing of the displacement of point C was observed, and the closing pressure was confirmed to be -5.96 cm H_2O. Note that this CT image for the tip adhesion case is from another patient.

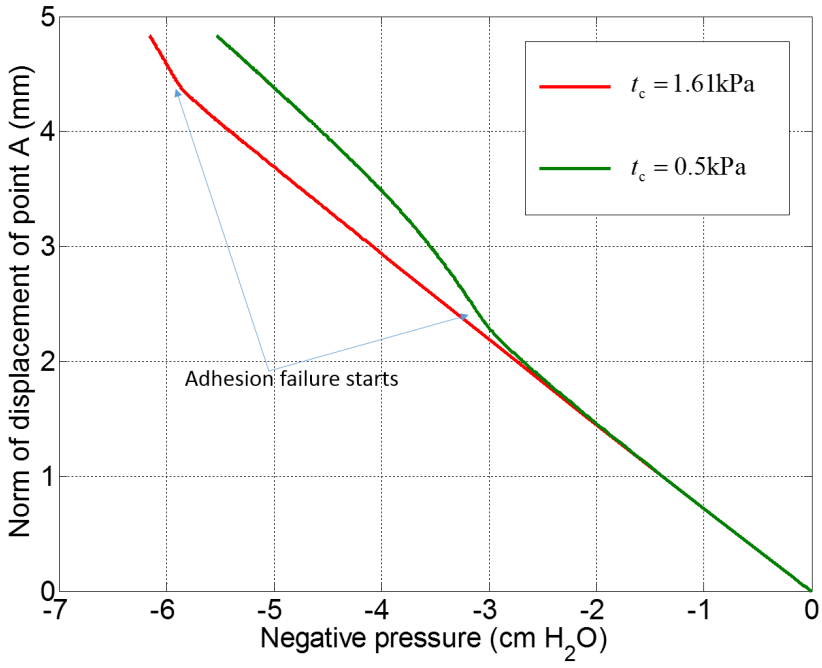

Fig. 9. Negative pressure against the norm of displacement of point A for the comparison of different critical traction stress cases. The length of the cohesive zone was set to be 70% soft palate length.